
# On predicting the turbulence-induced secondary flows using nonlinear k-ε models

G. Mompean, S. Gavrilakis, L. Machiels, and M. O. Deville

Citation: Physics of Fluids **8**, 1856 (1996); doi: 10.1063/1.868968

View online: http://dx.doi.org/10.1063/1.868968

View Table of Contents: http://scitation.aip.org/content/aip/journal/pof2/8/7?ver=pdfcov

Published by the AIP Publishing



# On predicting the turbulence-induced secondary flows using nonlinear $k$-$\epsilon$ models

G. Mompean,[a] S. Gavrilakis, L. Machiels, and M. O. Deville
*IMHEF-DGM, Swiss Federal Institute of Technology, 1015 Lausanne, Switzerland*

(Received 22 November 1994; accepted 6 March 1996)

Low turbulent Reynolds number direct simulation data are used to calculate the invariants of the Reynolds stress and the turbulent dissipation rate in a square duct. The results show that, depending on the region where the analysis is carried out, the turbulent flow field comes close to one-, two-, and three-component states. Modeling such flows—even at higher Reynolds numbers—will require models that can approach all three states. A number of related nonlinear $k$-$\epsilon$ models are tested *a priori* using the direct simulation data. The numerical simulation using Reynolds averaged Navier–Stokes equations with these models was performed. Their ability to predict the secondary flows, with a low-Reynolds $k$-$\epsilon$ model, cannot be gauged from realizability. © *1996 American Institute of Physics.* [S1070-6631(96)00807-0]

## I. INTRODUCTION

The assessment of turbulence models based on the Reynolds-averaged form of the equations of motion presents many difficulties that derive from the number and complexity of the underlying physical assumptions that are made to close the equations. The complications are compounded when the predictions of such models are to be compared with low-order flow statistics since, in addition to physical considerations, model predictions contain grid-resolution effects, convergence errors, and most significantly the explicit or implicit consequences of the chosen boundary conditions. These considerations make *a posteriori* evaluation of turbulence models an unreliable process. However, the evaluation of the assumptions used in the derivation of turbulence closures may be *assumed* to lead to rational expectations about the applicability of such models. The usefulness of this approach is also somewhat reduced since, in general, the physical assumptions that are made in the derivation of the various turbulence models are intended to make the analysis possible whereas the models are applied, even unmodified, to flows of different statistical properties. Moreover, some models, like those for the pressure strain terms, are inherently very difficult to test even when direct simulation databases are available.

One of the most widespread closure assumptions used in turbulence modeling is that of an eddy viscosity linking the deviatoric Reynolds stresses tensor linearly to the local mean strain. This type of closure is known to be incapable of predicting some well-established turbulent phenomena such as the effects of streamline curvature, rotation, and turbulence-induced secondary flows near corners.[1] Extensions of this type of model have been sought by including additional terms that are nonlinear functions of the mean flow strains. Speziale[2] was able to derive a nonlinear constitutive relation for the turbulent stresses by imposing form invariance for an arbitrary frame change in the limit of two-dimensional turbulence. In this model the expression for the Reynolds stress contains terms that are similar to those used for the laminar stress of a Rivlin–Ericksen fluid.[3] A similar set of constitutive relations has been derived from the invariance and realizability constraints,[4] renormalization group theory,[5] simplifying the modeled Reynolds-stress equation.[6] A discussion concerning the assumptions underlying this type of model is given in Gatski and Speziale,[7] who were also able to extend Pope's[8] earlier work and provide a framework for deriving explicit algebraic models.

In the present study the data from the direct simulation of a low Reynolds number turbulent flow through a straight square duct is used to describe the characteristics of the flow field within a quadrant, and to test the ability of several nonlinear eddy viscosity models to reproduce some of them. In the work by Huser *et al.*[9] the terms of the equations for each Reynolds stress components have been calculated, but it is the validity of the models for each of these terms—crucially the pressure strain—that are needed in order to gauge the applicability of the nonlinear algebraic stress models. In the approach taken herein the predictions of such models are tested in two ways. First, the data required by the models for each Reynolds stress evaluation is supplied from the DNS and their predictions are tested against the DNS data. Second, a set of predictions made by using the $k$-$\epsilon$ model for the turbulent scales are compared. These results are also compared with predictions from a full Reynolds stress model.[10] The aim being to not study the full Reynolds stress model (RSM) *per se* but to offer an additional set of comparisons. In Sec. II the turbulent flow field is described in terms of the invariants for the Reynolds stress and dissipation anisotropy tensors, the ratio of production to dissipation, and the mean vorticity equation. The nonlinear formulation for the Reynolds stresses derived by several authors,[1,4–7] which can produce the turbulence-induced secondary flows, are tested. This is done in Sec. III, first, by inserting all the necessary data calculated from the direct simulation data into the prescription for the Reynolds stresses and comparing the results with those from the direct simulation stresses. This approach is referred to as *a priori* testing and indicates the compatibility of the model inferred by constitutive relation with the Navier–Stokes equations at the Reynolds number of the

[a]On leave from Universidade Estadual de Campinas, FEM, DE, 13084-100 Campinas, SP, Brazil.

 1070-6631/96/8(7)/1856/13/$10.00 

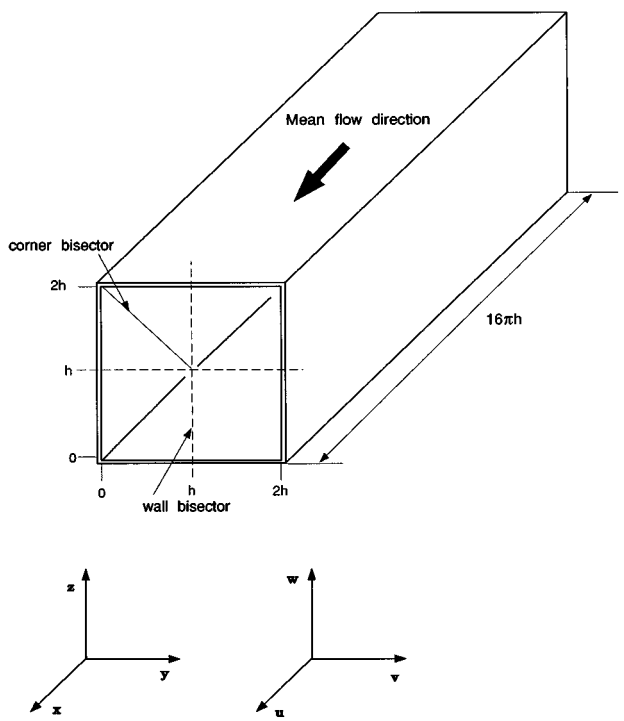


FIG. 1. Geometry and coordinate system.

simulation. In Sec. IV, the influence of the corner on the turbulent field is inspected and the use of a wall damping function is analyzed and considered for practical numerical computations. A second test is included, Sec. V, where the predictions based on the numerical solution of the Reynolds-averaged Navier–Stokes equations (RANS) with the different nonlinear stress models (using the $k$-$\epsilon$ equations for calculating the turbulent scales) are compared with the DNS data, differential Reynolds stress model (RSM)[10] calculations, and measurements.[11] Conclusions are drawn in Sec. VI.

## II. THE DIRECT SIMULATION

The basic flow statistics of the turbulent flow through a straight duct of square cross section at low Reynolds number are now available through a number of independent direct simulations of this bounded flow.[12–14] There is good qualitative agreement in the statistics extracted from these simulations, thus enabling the study of the duct flow with some confidence. The simulation database that will be used in this paper is that obtained by Gavrilakis in Ref. 14. Briefly, the main characteristics of the simulation are as follows. For spatial approximation of the Navier–Stokes equations, a mixed Fourier and finite difference approximation scheme is used. The flow variables are expanded into discrete Fourier series along the homogeneous streamwise direction $(x)$, Fig. 1, whereas second-order centered difference approximations are used for the inhomogeneous directions $(y,z)$. The disparate convergence properties of the two types of numerical approximation are partly offset by the unavoidable use of the largest grid spacing along the streamwise (Fourier) direction. This arises from the need to employ a relatively long domain

TABLE I. Numerical and physical parameters of the simulation: $\overline{U_0}$, mean centerline velocity; $U_m$, bulk velocity; $u_\tau$, average friction velocity over the duct perimeter; $\langle k\rangle$, volume and time-averaged turbulent kinetic energy; λ, Taylor microscale based on the streamwise velocity $u$.

| | |
|---|---|
| $\mathrm{Re}=\overline{U_m}2h/\nu$ | 4800 |
| $\mathrm{Re}^+=u_\tau 2h/\nu$ | 320 |
| Domain size in $x,y,z$ | $16\pi h\times 2h\times 2h$ |
| Grid size | $768(x)\times 127(y)\times 127(z)$ |
| Resolution in $\nu/u_\tau$ units | 10.5 in $x$; 0.48–4.6 in $y$ and $z$ |
| Length of flow sample | $4.4\ h/u_\tau$ |
| $\overline{U_0}/U_m$ | 1.33 |
| Friction factor | 0.036 |
| $\langle k\rangle/u_\tau^2$ | 2.2 |
| Maximum $\mathrm{Re}_\lambda$ | 205 |
| Centerline $\mathrm{Re}_\lambda$ | 32 |
| Maximum Kolmogoroff scale | $1.5\ \nu/u_\tau$ |

in the streamwise direction in order to secure sufficient decorrelation of the turbulent field. The time marching method is based on the second-order Adams–Bashforth scheme for all terms of the equations of motion. This allows the resolution of all convective and viscous time scales carried by the simulation and ensures that time stepping errors are negligible. The Reynolds number based on the mean flow velocity, $U_m$ (the overbar will henceforth be used to denote the ensemble average, which in the case of the simulation is assumed to be equivalent to streamwise, time, and octant averaging), and the duct hydraulic diameter is 4800. Additional data on the simulation are given in Table I.

The turbulent flow statistics required for assessing most nonlinear and algebraic stress models are the mean velocity field, $\overline{U_i}$, the Reynolds stress tensor $\overline{u_i u_j}$, and the dissipation rate $\epsilon$. Only the dissipation rate presents some difficulties in its extraction from the simulation. An implicit assumption of homogeneity of $\epsilon$ is made when it is commonly defined by

$$\epsilon=\nu\overline{\left(\frac{\partial u_i}{\partial x_j}\right)^2}, \tag{1}$$

in turbulence modeling (summation over recurrent subscripts is assumed). Calculations by Antonia *et al.*,[15] and more recently by Bradshaw and Perot,[16] have shown that definition (1) differs by a few percent from the exact dissipation rate,

$$\epsilon=\frac{1}{2}\,\nu\overline{\left(\frac{\partial u_i}{\partial x_j}+\frac{\partial u_j}{\partial x_i}\right)^2}. \tag{2}$$

The dissipation rate is here assumed to be given by the form (1) as it is commonly practiced in turbulence modeling. To obtain $\epsilon$ from the simulation, each component of the discretized momentum equation was multiplied by the appropriate velocity component and the terms involving viscosity were recast into terms involving stress–strain products of the form (1). This is the dissipation rate cell-averaged velocities, whereas direct differencing of definition (1) would be an approximation of that rate. Figure 2 shows the near-wall variation of $\epsilon^+(=\nu\epsilon/u_\tau^4)$ with $z^+(=u_\tau z/\nu)$, where $u_\tau$ is the friction velocity, along the wall bisector (see Fig. 1) and it is compared with the plane channel distribution from Kim *et al.*[17] Wall parameters are used to scale the variables from both simulations, but for the square duct data the value of the

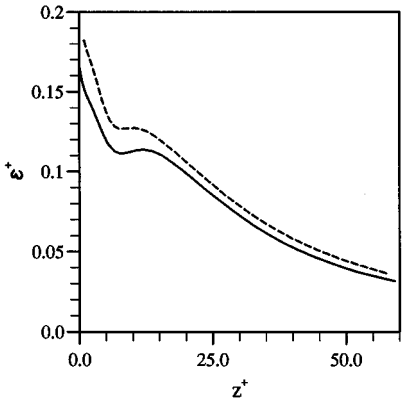


FIG. 2. Distribution of $\epsilon$ calculated from the DN simulations of a plane channel and the square duct: ---, square duct along the wall bisector; —, plane channel (Kim, Moin, and Moser[11]).

friction velocity, from the midwall $(0,h,0)$ has been used. For the present flow, estimates of the dissipation based on Eq. (2) were found to differ by at most six percent from the homogeneous value, in agreement with previous work.

The distribution of $\epsilon$ over one duct quadrant is shown in Fig. 3. The wall values of dissipation are nonzero everywhere, with the maximum values occurring at the center of each wall but decreasing monotonically toward zero at the corner. The near-wall minimum and maximum seen in Fig. 2 near $z^+=10$ are related to the oscillatory behavior of the contour lines near each wall. For either the $y=0$ or $y=2h$ wall (similar arguments can be applied to the other two walls by changing $v$ to $w$, $y$ to $z$ and $z$ to $y$), the near-wall dissipation rate is dominated by the terms $\overline{(\partial u/\partial z)^2}$ and $\overline{(\partial v/\partial z)^2}$ and somewhat away from the wall the $\overline{(\partial u/\partial y)^2}$ also becomes important. These terms also dominate the near-wall values of the fluctuating spanwise $(\omega_y)$ and streamwise

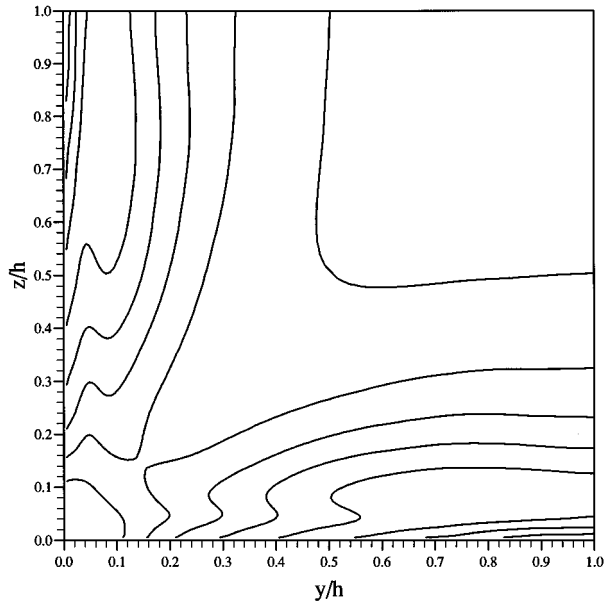


FIG. 3. Distribution of $\epsilon^+$ within a duct quadrant. DNS results—increment: $2.6\times10^{-2}$.

$(\omega_x)$ and normal $(\omega_z)$ vorticity components, respectively. (Note that the implied relation between the vorticity and dissipation fields occurring due to the presence of the corners is different to that deduced for high Reynolds number flows, as in Ref. 18). A component of these motions, those correlated to the fluctuating velocities gradients, contribute to the generation of mean vorticity, as it is evident from the equation for the mean streamwise vorticity $\Omega$ $(=\partial W/\partial y-\partial V/\partial z)$, which may be written in the form

$$\overline{V}\frac{\partial\Omega}{\partial y}+\overline{W}\frac{\partial\Omega}{\partial z}-\nu\,\nabla^2\Omega=\left(\overline{\omega_y\frac{\partial u}{\partial y}}+\overline{\omega_z\frac{\partial u}{\partial z}}\right)+\overline{\omega_x\frac{\partial u}{\partial x}}-\left(\frac{\partial}{\partial y}\overline{v\,\omega_x}+\frac{\partial}{\partial z}\overline{w\,\omega_x}\right),\quad(3)$$

where $\nabla^2$ the two-dimensional Laplace operator. Thus, in principle, a model would have to capture the effects of the near-wall anisotropy due to a subset of dissipative motions.

Since many turbulence closures are tested on predicting idealized turbulent flows, such as homogeneous shear flows, it is worth checking how well these conditions are met within the flow fields, which most closures ultimately aim to predict. Typically, nonlinear Reynolds stress models may be characterized by their ability to predict the secondary flows within a square duct—a relatively weak flow phenomenon driven entirely by the turbulent field. Aspects of the state of such turbulent field can be summarized by the map of the second and third invariants of the Reynolds stress and dissipation anisotropy tensors.[19] The Reynolds stress and dissipation rate anisotropy tensors are defined by

$$b_{ij}=\frac{\overline{u_iu_j}}{2k}-\frac{1}{3}\,\delta_{ij},\quad d_{ij}=\frac{\epsilon_{ij}}{2\epsilon}-\frac{1}{3}\,\delta_{ij},\qquad(4)$$

where $k\equiv\frac{1}{2}\overline{u_iu_i}$, $\epsilon_{ij}=2\,\nu\overline{u_{i,n}u_{j,n}}$, and $\delta_{ij}$ is the Kronecker delta. The second $(II_b,II_d)$ and third $(III_b,III_d)$ invariants (Ref. 19) are defined by

$$II_b=-\tfrac{1}{2}b_{ij}b_{ji},\quad II_d=-\tfrac{1}{2}d_{ij}d_{ji},\qquad(5)$$

and

$$III_b=\tfrac{1}{3}b_{ij}b_{jk}b_{ki},\quad III_d=\tfrac{1}{3}d_{ij}d_{jk}d_{ki}.\qquad(6)$$

Figures 4 and 5 show the variation of $-II$ against $III$ for the Reynolds stress and dissipation, respectively. Along the wall bisector the anisotropy in the Reynolds stress is most pronounced near $z^+=7$, whereas the dissipation rate is most anisotropic near $z^+=3$, where $z^+=zu_\tau/\nu$. This is in good agreement with the findings of Antonia *et al.*[15] Near the center of the duct the Reynolds stress and the dissipation reach an approximately isotropic state $II=III=0$. Some difference with the plane channel results is found away from the walls where the duct flow is closer to being axisymmetric as the invariants hug the right-hand side of the bounding triangle. Axisymmetry is also evident along the corner bisector. In the near-wall region of the wall bisector, the approximate two-dimensional state of the turbulence shows stronger anisotropy than the equivalent region in the plane channel. A region closely approximating one-component turbulence is found as the corner is approached $(-II_b=0.32,\ III_b=0.071$ at $y=z=0.013h)$, as shown in Fig. 5. The dynamics of the

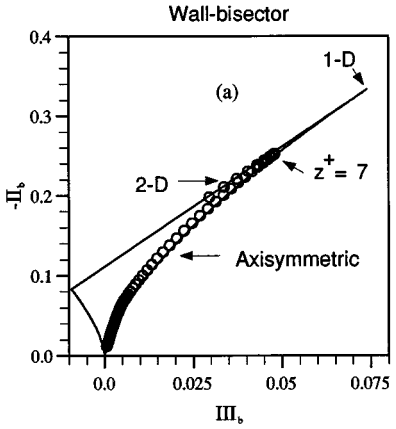


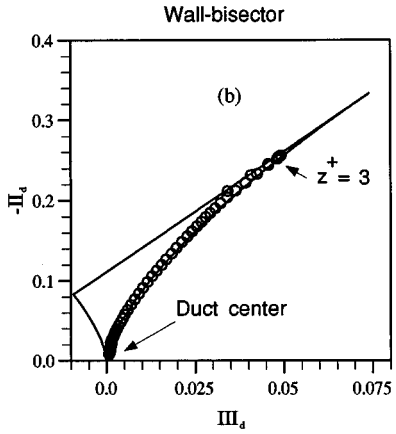


FIG. 4. Map of the second and third invariants along the wall bisector for (a) Reynolds stress anisotropy tensor; (b) dissipation rate anisotropy tensor.

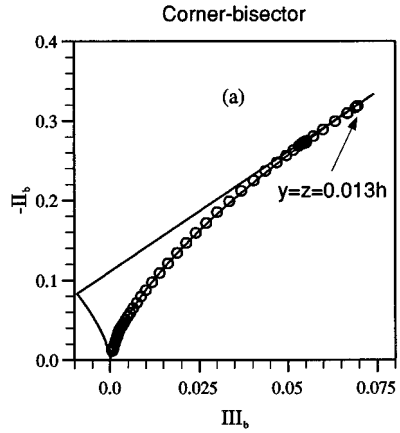


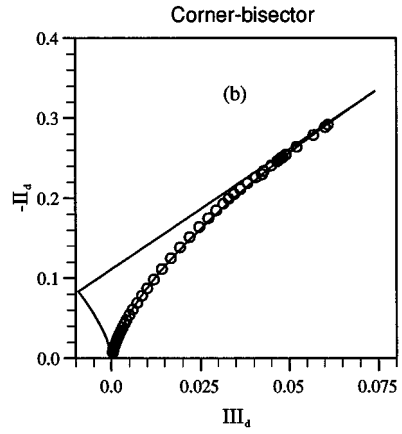


FIG. 5. Map of the second and third invariants along the corner bisector for (a) Reynolds stress anisotropy tensor; (b) dissipation rate anisotropy tensor.

near-corner flow is therefore fundamentally different from those in the rest of the duct, and although these two types of turbulent flow are in contact, the structures present within each region are uncorrelated.[20] Thus, square duct flow regions approximating one-, two-, and three-component turbulence are found within each quadrant and hence any Reynolds stress closure that does not depend on the use of artificial boundary conditions must be able to approach all three states.

The relationship between the diagonal components of the anisotropy tensor $d_{ij}$ and $b_{ij}$ along two lines parallel to one set of walls is shown in Figs. 6. The relation between these components appears to be approximately linear ($d_{11} \simeq b_{11}$, $d_{22} \simeq b_{22}$, $d_{33} \simeq b_{33}$), both along the wall bisector and on lines parallel to it. As the corner is approached the points of $b_{ij}$ and $d_{ij}$ tend to cluster around $d_{11} \simeq b_{11} \simeq \frac{1}{2}$ and $d_{22} \simeq b_{22} \simeq d_{33} \simeq b_{33} \simeq -\frac{1}{4}$.

The terms in which the origin of the secondary flows may be sought depend on the form of the dynamical equation that can be studied. The emphasis on the normal stress anisotropy is due to the relatively simple form of the equation for the mean vorticity and to the absence of pressure terms. But, Gessner,[21] and more recently, Huser and Biringen[12] have advanced arguments based on the imbalances of mean and turbulent energy in the flow field, respectively. In Fig. 7 the distribution of the ratio of turbulent energy production rate $P$ to the dissipation rate $\epsilon$ is shown. The local equilibrium condition ($P \approx \epsilon$) is valid over a small fraction of the flow cross section only and therefore cannot serve in modeling this flow. In contrast, the distribution of the various local minima and maxima suggests that the turbulent energy imbalance may be driving the secondary flows. The local dissipation exceeds the production in the vicinity of the corner bisector over most of its length, except for a relatively thin region near the corner. The local minimum at $y^+ = z^+ \approx 50$, $P/\epsilon \approx 0.2$, is due to very low values of $P$. One contributing factor for this minimum in $P$ has been suggested by the mode analysis of the near-corner turbulent flow (Gavrilakis[14]), which shows that the Reynolds-averaged turbulent production term may contain both positive and negative contributions. This is due to the kinematic constraints on the flow in the near-corner region, and may also help to explain the observed drag reduction in turbulent flows over riblets aligned with the mean flow. On either side of the local minimum and close to each wall a maximum is found with $P/\epsilon > 2$. The distance of each maximum from the corner appears to be about the same as the distance of the maximum of mean streamwise vorticity, which was found on the corner

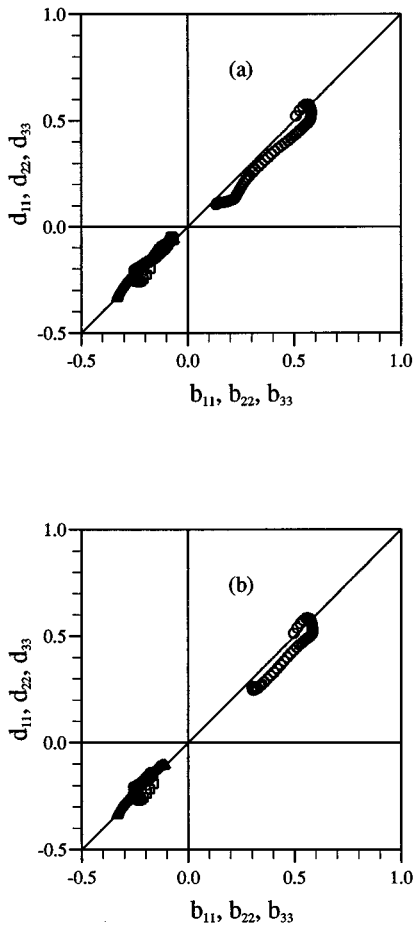


FIG. 6. Relationship between the anisotropic tensors of the dissipation and Reynolds stress for the diagonal terms. (a) Wall bisector; (b) parallel line to the wall bisector close to the corner ($y/h=0.3$); ○, $d_{11}$ vs $b_{11}$; □, $d_{22}$ vs $b_{22}$; △ $d_{33}$ vs $b_{33}$.

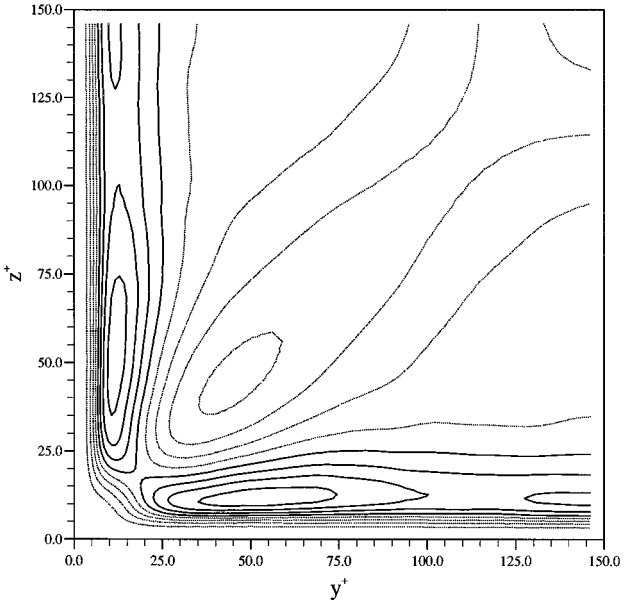


FIG. 7. Distribution of the ratio between the turbulent energy production and dissipation, ····, $P/\epsilon<1.0$ and —, $P/\epsilon>1.0$. The maximum of $P/\epsilon$ is 2.25, and the minimum at $y^+=z^+=50$ is $P/\epsilon=0.2$.

walls (Gavrilakis[13]). The proximity of the two extrema in $P/\epsilon$ near the corner, the direction, and magnitude of the mean secondary velocity in that area imply that the turbulent energy transport from the wall toward the bisector is dominated by turbulent convection and pressure diffusion. These two processes will become relatively less important away from the corner, as the separation between the region of $P/\epsilon>1$ near the wall and that of $P/\epsilon<1$ near the wall bisectors become increasingly separated. The $P/\epsilon$ ratio tends to zero toward the duct centerline.

## III. THE ALGEBRAIC STRESS MODELS

Evaluations of the terms in the equation for the mean streamwise vorticity,[12,13] have shown that three terms are involved in its generation, namely gradients of the normal cross-stream stress difference, gradients in the secondary stress, and viscous diffusion of the mean vorticity. Emphasis is usually placed on the normal stress anisotropy, which is somewhat misplaced, since there are other equally important terms, and the normal stress anisotropy *per se* does not lead to the generation of secondary flows; one has to achieve correct modeling for the gradients of anisotropy. The maxima of these terms occur close to the corner walls, where the influence of viscosity cannot be neglected. It is therefore very likely that accurate and reliable predictions of the secondary flows in the vicinity of the corner cannot be achieved without the explicit inclusion of the effects described. Also, in view of the significance of the viscous terms near the corner, the extension of the high Reynolds number models to include viscous effect is essential. Presently, Reynolds stress closures consistently underestimate the magnitude of the secondary flows in square ducts.

There seems to be no satisfactory low Reynolds number version for the $k$-$\epsilon$ model,[4] and thus comparison between different algebraic stress models is only possible if the values for the mean strain, $k$ and $\epsilon$ from the direct simulation of the square duct flow, are used to calculate the Reynolds stresses prescribed by each model. One of the main features of the model of Speziale,[2] hereafter referred to as the $S$ model, is its ability to predict the turbulence-induced secondary flows—albeit at high Reynolds numbers—and is one of those tested herein. According to this model the Reynolds stress $-\overline{u_i u_j}$ is given by

$$-\overline{u_i u_j}=-\frac{2}{3}k\delta_{ij}+c_\mu\frac{k^2}{\epsilon}2D_{ij}+C_D c_\mu^2\frac{k^3}{\epsilon^2}\times\left(D_{im}D_{mj}-\frac{1}{3}D_{mn}D_{mn}\delta_{ij}\right)+C_E c_\mu^2\frac{k^3}{\epsilon^2}\times\left(\mathring{D}_{ij}-\frac{1}{3}\mathring{D}_{mm}\delta_{ij}\right), \tag{7}$$

where $D_{ij}=(\overline{U_{i,j}}+\overline{U_{j,i}})/2$ is the mean strain tensor, $\mathring{D}$ is the upper-convected derivative of $D$, defined as follows:

$$\mathring{D}_{ij}=\frac{\partial D_{ij}}{\partial t}+\overline{\mathbf{U}}\cdot\boldsymbol{\nabla}D_{ij}-\frac{\partial\overline{U_i}}{\partial x_k}D_{kj}-\frac{\partial\overline{U_j}}{\partial x_k}D_{ki}. \tag{8}$$

TABLE II. Coefficients for different nonlinear algebraic stress models.

| | $F_1$ | $F_2$ | $F_3$ | $c_\mu$ |
|---|---|---|---|---|
| Demuren and Rodi | 0.052 | 0.092 | 0.013 | 0.09 |
| Rubinstein and Barton | 0.104 | 0.034 | −0.014 | 0.0845 |
| Shih, Zhu, and Lumley | $-4/A$ | $13/A$ | $-2/A$ | $0.67/(1.25+\eta)$ |
| Gatski and Speziale | $0.030R$ | $0.093R$ | $-0.034R$ | $0.680R$ |

$A=1000+\eta^3$
$R=(1+0.0038\eta^2)/D$
$D=3+0.0038\eta^2+0.0008\eta^2\zeta^2+0.2\zeta^2$

The constants $C_D$ and $C_E$ were estimated by Speziale[2] to be 1.68, whereas $c_\mu$ is normally set to 0.09.

A group of related nonlinear algebraic stress models derived from different types of analysis may be summarized as

$$-\overline{u_i u_j}=-\frac{2}{3}k\delta_{ij}+c_\mu\frac{k^2}{\epsilon}2D_{ij}-F_1\frac{k^3}{\epsilon^2}\times\left(\overline{U}_{i,n}\overline{U}_{n,j}+\overline{U}_{j,n}\overline{U}_{n,i}-\frac{2}{3}\overline{U}_{m,n}\overline{U}_{n,m}\delta_{ij}\right)-F_2\frac{k^3}{\epsilon^2}\left(\overline{U}_{i,n}\overline{U}_{j,n}-\frac{1}{3}\overline{U}_{n,m}\overline{U}_{n,m}\delta_{ij}\right)-F_3\frac{k^3}{\epsilon^2}\left(\overline{U}_{n,i}\overline{U}_{n,j}-\frac{1}{3}\overline{U}_{n,m}\overline{U}_{n,m}\delta_{ij}\right). \tag{9}$$

These are the models of Shih, Zhu, and Lumley[4] (hereafter referred to as SZL), Rubinstein and Barton[5] (RB), Demuren and Rodi[6] (DR), and Gatski and Speziale[7] (GS). The factors for each model are given in Table II.

All constants are presumed to be appropriate for high Reynolds number flows. In the SZL model the coefficients of the nonlinear terms are functions of the ratio of turbulent to mean-strain time scales, defined by

$$\eta=\frac{k}{\epsilon}(2D_{ij}D_{ij})^{1/2}. \tag{10}$$

The GS model contains the parameter $\zeta$, namely the ratio of turbulent to vorticity time scales, defined by

$$\zeta=\frac{k}{\epsilon}(w_{ij}w_{ij})^{1/2}, \tag{11}$$

where $w_{ij}=(\overline{U}_{i,j}-\overline{U}_{j,i})/2$ is the vorticity tensor.

It is also noted that the general form of Eq. (9) can be found in the Speziale model, Eq. (7), by neglecting the advection transport term $(\mathbf{U}\cdot\boldsymbol{\nabla})$ in the Oldroyd derivatives. No attempt was made here to optimize the values of the coefficients for the low Reynolds number flow under study, since their wider validity could not be determined. It is expected, however, that improved agreement in the low-order statistics between the models and the direct simulation may be achieved by some other choice for the constants. The essential characteristics of each model are still discernible, with the set established by the authors of the models. In Fig. 8, a comparison between the model estimates and the direct simulation results for the three normal intensities along the wall bisector is shown. The results from the models show good agreement with the simulation for $z^+>70$, whereas

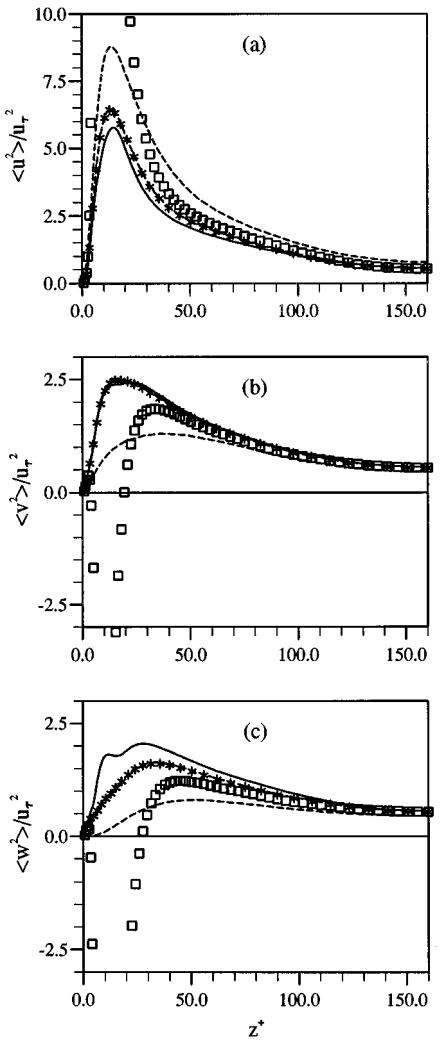


FIG. 8. Turbulent intensities along the wall bisector: ---, DNS square duct; -*-, Gatski and Speziale[7] *a priori* test; —, Shih, Zhu, and Lumley[4] *a priori* test; □, Speziale[2] *a priori* test.

substantial differences are found near the walls. The Speziale model gives negative cross-flow intensities for $z+<30$ (where the flow approaches the two-component limit), whereas the $\overline{u^2}$ component reaches very high values $(40u_\tau^2)$, so that the sum of the three components remains equal to $k$. The negative values are for the greater part due to the Oldroyd derivatives in the model. Although it has been recognized that the Speziale model is not strongly realizable, the normal intensity components are known to be important in the generation of the secondary flows and thus realizability in all the components would be desirable. The negative values for $\overline{v^2}$ and $\overline{w^2}$, not shown, persist all around the duct boundaries. Interestingly, when using these negative values to estimate the anisotropy source term for the equation of the mean streamwise vorticity, $\Omega$ (not shown), it turns out that this generation term has, at least, the correct sign within each octant.

The near-wall intensities calculated from the SZL and GS models are all positive, and remain so throughout the duct cross section, but they tend to be much more isotropic. The maximum in $\overline{u^2}$ of the SZL and GS models underesti-

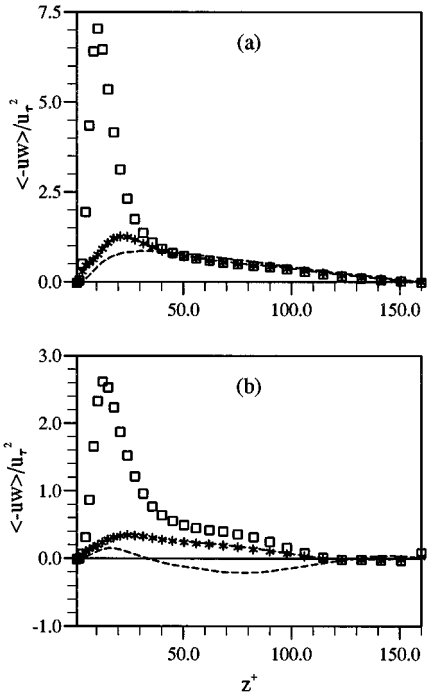


FIG. 9. The Reynolds stress $\overline{uw}/u_\tau^2$, (a) along the wall bisector, (b) near the corner bisector ($y/h=0.14$): ---, DNS square duct; --*--, Gatski and Speziale[7] *a priori* test; □, Speziale[2] *a priori* test.

mates the simulation value by more than 30%, whereas the near-wall cross-stream intensities are overestimated by about a factor of 2, the GS model gives values for $\overline{u^2}$ close to DNS. The asymptotic behavior of each predicted intensity as the wall is approached (in the viscous sublayer) is $2k/3$. This term dominates for $z^+<2$, where $u^+\sim z^+$ and the locally spanwise component varies as $z^+$. This is not surprising since these algebraic models were derived for high Reynolds number flows. However, the most important nonlinear contributions to the Reynolds stresses of these models are essentially confined to $2<z^+<50$—a region that normally is not resolved in the modeled flows. Thus, the good agreement between the models and the simulation for $50<z^+$ is only in small part due to the extra modeling effort. It is also worth mentioning that the stresses of the models by Rubinstein and Barton,[5] Demuren and Rodi,[6] were also found to give negative intensities in the near-wall region of the square duct.

Figure 9 compares the model values for the Reynolds shear stress $\overline{uw}$ with the results of the simulation along the wall bisector and near the corner bisector. Both models give numerically higher values for this quantity. The GS model differs the least, by a factor of 2, from the simulation, which may seem consistent with its prediction of much higher values for the peak $\overline{w^2}$, but it also underpredicts the streamwise component of the intensity in the same region. The behavior of the *S* model is much harder to interpret, giving a peak value for $\overline{uw}$ of about an order of magnitude larger. Both models predict peak values much closer to the duct wall with implied production rates for the turbulent kinetic energy substantially higher than the dissipation rates obtained with the DNS. Thus, a calculation using the $k$-$\epsilon$ model must overestimate the local dissipation rate in order to recover the correct mean flow profile. Closer to the corner, Fig. 9(b), the near-wall behavior of the modeled $\overline{uw}$ is similar to that near the wall bisector, but the quantitative differences have increased. The *S* and the GS model never changes sign as the simulation data does in the region $30<z^+<130$.

## IV. CORNER DAMPING FUNCTION

In view of the complexity of the effects of the corner geometry on the turbulent field, it would be expected that the most used $k$-$\epsilon$ two-equation model should be adapted for this type of boundary influence, even when the model solution is not carried to the boundaries. This is rather difficult at present since the small-scale (dissipation) physics of the flow is not fully captured by any of the current simulations. However, a number of mean effects on the turbulent field can be observed, and need to be modeled. Those include the variation of the boundary values of $\epsilon$ between a finite maximum at the midwall and the zero at the corner; dissipation rate anisotropy (also see Ref. 22); the negative energy production contribution in the $k$ equation;[14] and kinematic blocking[23] of turbulence near the corner. It is interesting to know whether the existing algebraic stress models can be modified to account for near-wall effects to improve the agreement with the simulations and experiments. This is usually attempted in part, by inserting a function $f_\mu$ in the definition for the eddy viscosity to account for the near-wall damping influences, thus

$$\nu_t = c_\mu f_\mu \frac{k^2}{\epsilon}, \tag{12}$$

where $c_\mu$ is a constant whose value here will be taken to be 0.09. The point values of $f_\mu$ are calculated by inserting the values of $k$, $\epsilon$, and the strain rate in Eq. (9). This equation allows the calculation of the eddy viscosity, and hence $f_\mu$ using the form (12) in a number of different ways. In order to make the formula for the square duct compatible with the calculation of Rodi and Mansour[24] for a plane channel, the following formulation has been adopted:

$$f_\mu = \frac{1}{c_\mu}\frac{(\overline{uv})^2+(\overline{uw})^2}{k^2}\frac{\epsilon}{P}. \tag{13}$$

The exact form of this term depends on the type of model used for the turbulent stresses, but the contribution due to the terms linear in $D_{ij}$,

$$P=\overline{uv}D_{12}+\overline{uw}D_{13},$$

is always present. It should be noted that for the flows with a three-dimensional mean flow field the turbulence production term will contain contribution involving all Reynolds stress components. For the present flow the terms of *P* shown above contribute overwhelmingly to the total production. For the nonlinear models, *P* has additional terms arising from the nonlinear part of the strain rates. Figure 10 shows the variation of $f_\mu$ along the wall and corner bisectors calculated by the linear and SZL models (the $f_\mu$ due to the other models has not been computed since they give rise to negative normal stresses). It appears that the distribution of values for the

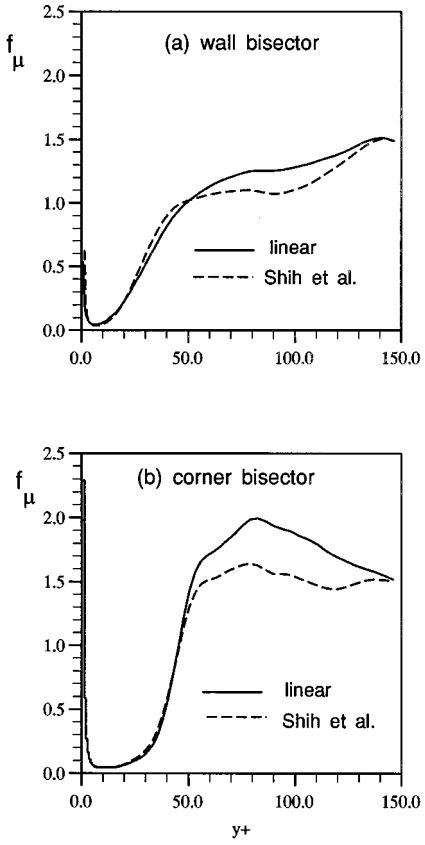


FIG. 10. Distribution of $f_\mu$ obtained with the linear and Shih, Zhu, and Lumley[4] models using DNS data.

former model may be fairly approximated by a constant of order one for $y^+$ or $z^+>60$. The nonlinear model of SZL is found to lead to nearly constant values for $f_\mu$ along the corner bisector but continuously increasing from the boundary along the wall bisector. For $y^+$ or $z^+<50$ the values from both models decrease sharply toward zero but for very small distances from the walls the values for $f_\mu$ diverge because the $\epsilon/P$ ratio diverges at the boundaries. Near the corner this function suggests considerable damping of the turbulent field up to about $y^+=z^+=40$—with a somewhat larger region for the nonlinear model. This corresponds closely to the finding of Gavrilakis[20] that the turbulent field in the region from the wall to $y^+=50$, $z^+=50$ is only weakly correlated with the flow field farther away from the corner. This is in contrast to the standard near-wall turbulent flow where velocity correlations are found to extend from the viscous sublayer to beyond the buffer layer. This implies that the flow just beyond the near corner region cannot be modeled in the way current for boundary layer-type flows. The elliptic boundary conditions proposed by Durbin[23] probably need to be extended to this type of calculation.

An attempt was made to use the values of $f_\mu$ derived from the direct simulation into a modeled simulation of this flow at the same Reynolds number, using in turn each of the constitutive relations shown in Table II, in conjunction with the RANS equations and the $k-\epsilon$ model of turbulence. A grid identical to that of the direct simulation was used and the values for the $f_\mu$ derived from it were assigned to the grid of the model calculations. This type of computation did not converge to a steady state. It appears that it may be unlikely for simple adjustments of the eddy viscosity near the boundaries to be sufficient.

A second attempt was made to use the models based on Eqs. (7) and (9) and Table II with the $k-\epsilon$ model in which the effects of the corner were accounted for qualitatively only through the use of damping wall functions. The numerical approximation of the RANS equations of motion was obtained through the standard finite volume techniques on a staggered grid, where the pressure is defined at the center of every cubical grid and the velocity components at the center of every face. The normal Reynolds stress are cell centered, while the off-diagonal terms are located at the mid-edges. A number of different upwind approximation schemes were tried for representing the nonlinear terms, but no sensitivity was detected from this part of the algorithm. The solution to the equation was obtained by advancing explicitly in time the equations of motions until a steady state was reached, while enforcing the continuity at each step through the solution of the discrete Poisson equation for the pressure. Details of the algorithm are given in Mompean.[25] The computational domain in this type of calculation was one quadrant of the full duct while enforcing symmetry conditions along the symmetry axes of the flow. Typical grids were $41\times41$ points in the (quadrant) cross section. The results were found to be grid independent and insensitive to the initial conditions. The first grid point near the wall was always at $y^+<1.0$, when using the nonlinear models. Details of the turbulence model ($k-\epsilon$) and boundary conditions used can be found in Appendix A. The code and models (linear and nonlinear) were tested against the well-established plane channel results and gave good agreement.

A number of existing suggestions about modifying the near-wall eddy viscosity definition were tested. They were originally developed for plane boundaries (Chien;[26] Lam and Bremhorst,[27] Reynolds,[28] and Lindberg[29]), but it was found that the following relationship for $f_\mu$ produced results closer to the direct simulation:

$$f_\mu=[1-\exp(-0.08y^+)][1-\exp(-0.08z^+)]. \qquad (14)$$

The relationship provided high damping in the near corner region, where suppression in the turbulence due to the corner was observed in the direct simulation. This relation was independently used by Nisizima[30] when modeling the square duct turbulent flows at high Reynolds numbers.

## V. NONLINEAR AND FULL REYNOLDS STRESS PREDICTIONS

It would be expected that the full Reynolds stress model (RSM) give more accurate results, because important physical effects like convection and production are directly taken into account in the equations. Presently, the closures of the unknown terms in the RSM for a low Reynolds number are not well established. This is the subject of intensive ongoing research.[31] A recent paper from Naimi and Gessner[32] presents a modified form of the Launder, Reece, and Rodi[33] pressure–strain model. Theirs is applied for high Reynolds numbers in a square duct flow (65 000 and 250 000, based on

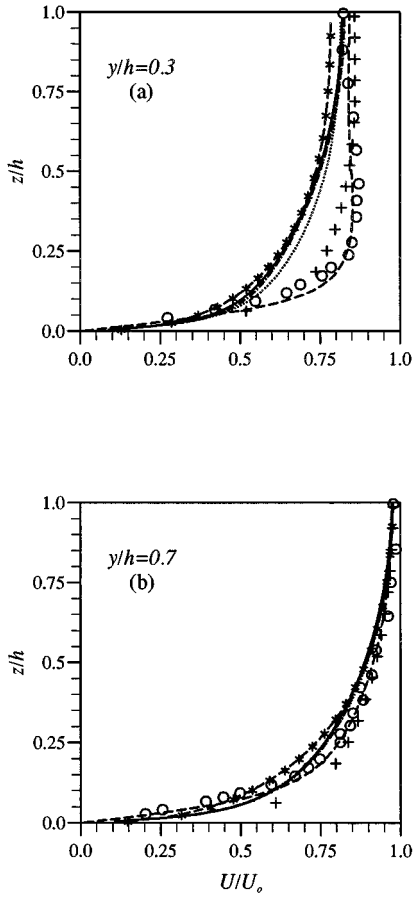


FIG. 11. Mean streamwise velocity profiles along two duct sections from the Reynolds-stress closure calculations; (a) $y/h=0.3$, (b) $y/h=0.7$, —, Shih, Zhu, and Lumley;[4] -·-, Rubinstein and Barton;[5] ⋯, Speziale;[2] --*--, Gatski and Speziale;[7] · · ·, linear model; +, RSM; ---, DNS square duct; ○, measurements of Cheesewright, McGrath, and Petty.[11]

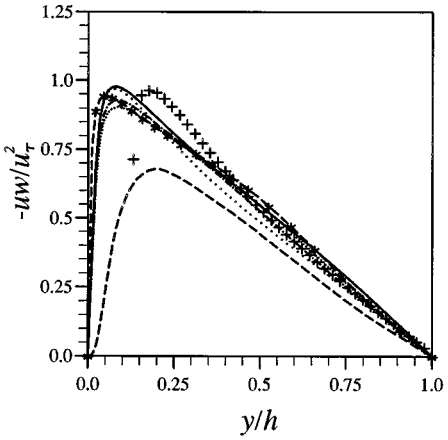


FIG. 12. The Reynolds stress $\overline{uw}/u_\tau^2$ from model calculation, DNS, and experiment along the wall bisector: —, Shih, Zhu, and Lumley;[4] -·-, Rubinstein and Barton;[5] ⋯, Speziale;[2] --*--, Gatski and Speziale;[7] · · ·, linear model; +, RSM; ---, DNS square duct.

the bulk velocity and on the height of the duct). Their results also underpredict the secondary flow in the region where the flow is fully developed. The prediction of a RSM is included in this work, and the results are compared with the predictions of the algebraic nonlinear $k-\epsilon$ model. The differential equations for the RSM were solved using the numerical method described above. The closures proposed by Gibson and Launder[10] were employed to obtain the unknown terms, viz. pressure–strain, turbulent diffusion, and dissipation. Details are given in Appendix B. In this model the assumption of high Reynolds number was used where the dissipative motions were assumed to be isotropic. To eliminate the uncertainty that the boundary conditions can provoke in the solution of the RSM equations, all the values for the Reynolds stress components and for $\epsilon$ were obtained interpolating DNS data; these values were used over the quadrant duct perimeter at $y^+\cong 10$.

The profiles of the mean streamwise velocity ($\overline{U}$) along two vertical sections ($y/h=0.3$ and 0.7) are shown in Fig. 11. Eight sets of results are compared; four of the nonlinear models (SZL, RB, S, GS), the linear $k-\epsilon$ model, the RSM, the DNS, and the measurements of Cheesewright, McGrath, and Petty.[11] At the section $y/h=0.3$, the DNS data and the measurements show a strong distortion on the mean velocity, whereas all nonlinear algebraic models are unable to predict this distortion on $U$. The RSM results show a good agreement with the DNS and measurements for the mean streamwise velocity. This may be due to the convective effect incorporated in the RSM.

Figure 11(b) shows the comparison near the wall bisector, the agreement for $U$ is good. This is not surprising since the $k-\epsilon$ model is known to reproduce accurately the mean flow of the infinite parallel channel turbulent flows. This also indicates that the present version of this model produces accurate results for the low Reynolds number channel flows.

The Reynolds stresses obtained with the nonlinear models differ substantially. All models give Reynolds stresses significantly larger than those found in the direct simulation (Fig. 12). Very close to the wall the nonlinear algebraic $k-\epsilon$ models predict a steeper rise of the $-\overline{uw}$ and much higher values for the peak than the simulation. The prediction given by the RSM is also overestimated for $-\overline{uw}$, but with the peak in the same position ($y/h=0.2$) as the DNS.

The comparison between the models, DNS data, and measurements for the spanwise velocity ($V$) for two vertical sections, $y/h=0.3$ and 0.7, is presented in Figs. 13(a) and 13(b). There is good qualitative agreement among the various datasets, and in particular, good agreement is found in the position of the zero crossings. This would suggest that the predicted positions of the secondary vortices within each octant are broadly similar (see Figs. 14 and 15). However, the differences between DNS and model results on the position of the extrema of the vorticity are at most 20%. Differences in the magnitude of the secondary velocities are greater, particularly for the maximum values of the secondary velocities near the duct walls. These differences can be large, depending on the model used. In Fig. 13(a) the difference between the $S$ model and the DNS at the extreme of $V$ is about 50%. The GS model gives very good agreement between the predictions and measurements for both sections ($y/h=0.3$ and 0.7)—the maximum error in the measured secondary velocity is less than 10%.[11] Among the nonlinear

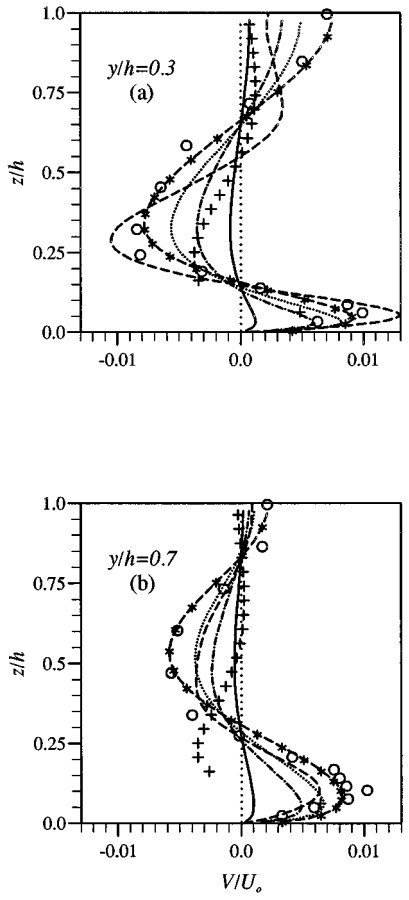


FIG. 13. Mean spanwise velocity profiles along two sections: (a) $y/h=0.3$, $y/h=0.7$, —, Shih, Zhu, and Lumley;[4] -·-, Rubinstein and Barton;[5] ···, Speziale;[2] --*--, Gatski and Speziale;[7] · · ·, linear model; +, RSM; ---, DNS; ○, measurements of Cheesewright, McGrath, and Petty.[11]

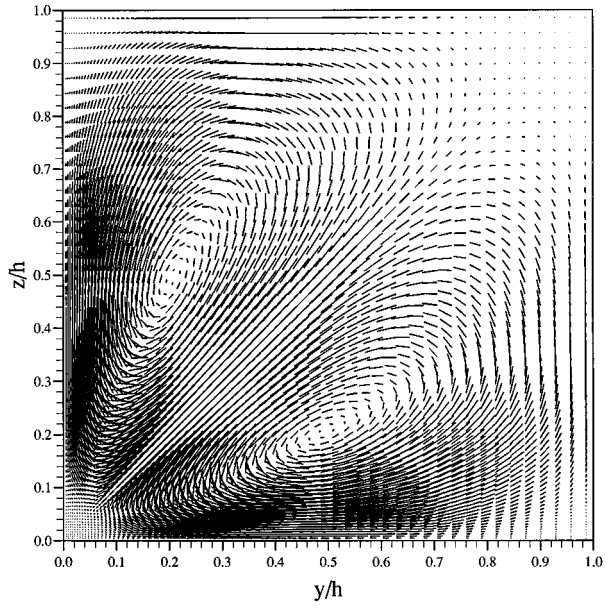


FIG. 14. Secondary velocity vectors in a quadrant obtained from DNS.

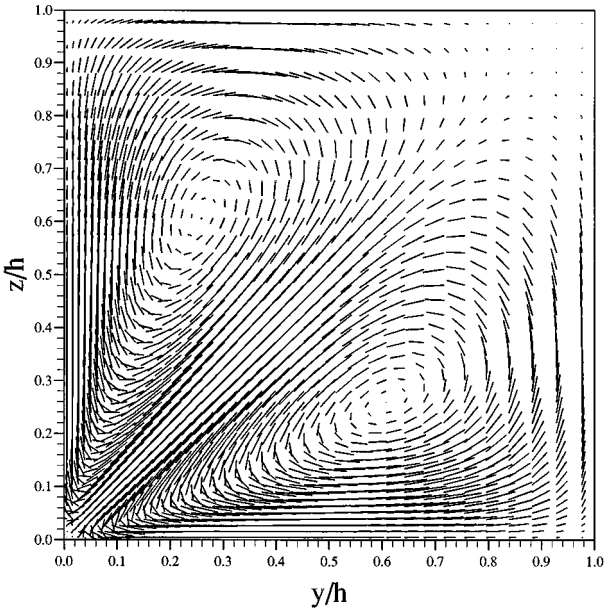


FIG. 15. Reynolds stress closure prediction of the secondary velocity in a quadrant. The constitutive relation is that proposed by Gatski and Speziale.[7]

models, the GS gives the best overall agreement with the simulation results. The SZL model that is realizable leads to very weak secondary flows. This can be attributed to the greater normal-stress isotropy seen in Sec. III above. Better agreement in the horizontal velocity profiles is found closer to the wall bisector (except for the SZL model), Fig. 13(b). This may not be unexpected since all models comply with the symmetry requirement of $V=0$ on the wall bisector.

The RSM predictions for the spanwise velocity show a weaker secondary flow than the DNS at the section $y/h=0.3$, Fig. 13(a), the magnitude is of the same order as the *S* and RB models predictions. At $y/h=0.7$, Fig. 13(b), the magnitude is correctly predicted, but the position of maximum negative velocity is misplaced.

Unlike the *a priori* tests, the intensities of the converged solution obtained with the above models are positive everywhere. The variations of root-mean-square fluctuating velocities along the wall bisector are shown in Fig. 16. In general, all nonlinear algebraic models fail to capture the anisotropy evident in the DNS results, even at the center of the duct. Indeed, the models overestimate the cross-stream intensities. The SZL model is closer to the linear eddy viscosity model, whereas the S, GS, and RB models predict a somewhat greater anisotropy. All nonlinear models underpredict the DNS peak of $u_{\mathrm{rms}}$ by at least 30%, whereas they overpredict the peaks in the cross-stream intensities by at least 20%. The best agreement with the DNS predictions for the turbulent intensities is obtained with the RSM.

The near-wall extrema of the $w_{\mathrm{rms}}$ from the RB and *S* models are due to their greater sensitivity on the local value of the dissipation rate (through the eddy viscosity); see Fig. 2. On the wall bisector the RB, DR, and SZL models may be written as

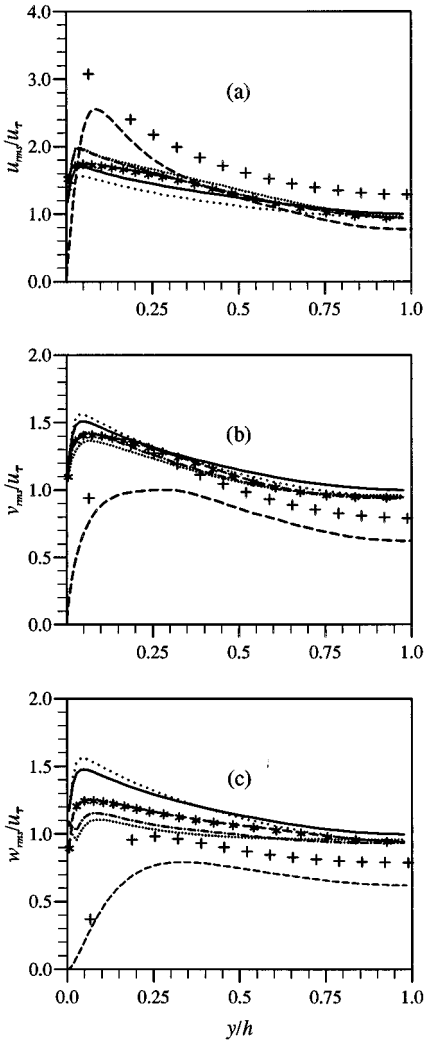


FIG. 16. Turbulence intensity profiles from the calculations using the nonlinear models and DNS along the wall bisector. —, Shih, Zhu, and Lumley;[4] -·-, Rubinstein and Barton;[5] ⋯ , Speziale;[2] --*-- Gatski and Speziale;[7] · · ·, linear model; +, RSM; ---, DNS.

$$\overline{w^2} = \frac{2}{3}k - (F_2 - 2F_3)\frac{k^3}{\epsilon^2}\left(\frac{\partial \overline{U}}{\partial z}\right)^2, \tag{15}$$

where the value of $(F_2 - 2F_3)$ determines the difference from the isotropic value for each model. Of the three models the SZL yields the smallest value for this factor.

The distribution of $\Omega$ from the DNS in Ref. 13 and the GS model are compared in Fig. 17. The DNS results are shown on the right side of the diagonal, and the GS model results on the left side. The results based on the GS model show that intense near-wall vorticity is due to the fact that the secondary velocity maximum occurs closer to the wall than in the DNS. Overall the mean vorticity maxima differ by about 10%, but the respective distributions are quite different.

## VI. CONCLUSIONS

The results from the direct numerical simulation in a square duct at the Reynolds number of 4800, based on the hydraulic diameter and bulk velocity, have been used to evaluate aspects of the turbulent flow that are involved in modeling near-wall flows. Maps of the second and third invariants for the Reynolds stress and dissipation anisotropy tensors indicate that within a quadrant the turbulent field comes close to one-, two-, and three-component states. There are many similarities between the duct flow along the wall bisector and the plane channel results. However, plane channel data are not helpful to model the flow close to the corners. The dynamics of the streamwise intensity enter directly in the equation for the generation of $\Omega$. No simple approximate relationship between the Reynolds stress and dissipation anisotropy tensors is apparent over the whole of the duct cross section.

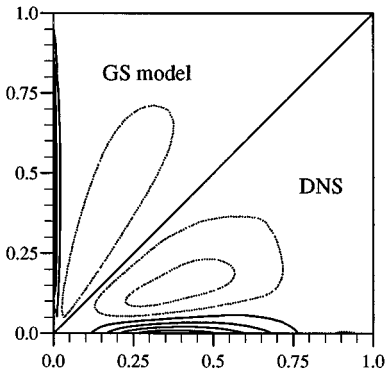


FIG. 17. Mean streamwise vorticity $\Omega$. Gatski and Speziale[7] model results (left side of the diagonal) and DNS square duct (right side). Continuous lines represent positive values; dotted lines negative values. Increment 2.0 $(u_\tau/h)^2$.

Several nonlinear $k$-$\epsilon$ models for the Reynolds stresses were tested *a priori* using the direct simulation data. The flow prediction of the nonlinear algebraic $k$-$\epsilon$ models were compared with the results of a full Reynolds stress model, DNS data, and measurements. These models were designed for high Reynolds numbers. Of all the nonlinear models tested, the one by Shih, Zhu, and Lumley[4] and by Gatski and Speziale[7] are strongly realizable, but in general, they underestimate the anisotropy between the three anisotropy components. The model of Speziale[2] shows negative cross-stream intensities near the duct walls. However, this aspect of the models cannot be correlated with their ability to predict the mean secondary flows when used with the RANS equations and the $k$-$\epsilon$ model. In this type of test the Gatski and Speziale[7] model performed best, but its results are in a limited qualitative agreement with the direct simulation data.

## ACKNOWLEDGMENTS

Dr. T. B. Gatski (NASA Langley Research Center) contributed for some helpful comments on the explicit algebraic stress models. Also, a number of constructive comments were contributed by the anonynous referees. G. Mompean would like to thank the Fundação de Amparo a Pesquisa do Estado de São Paulo (FAPESP) for the financial support during this study. The participation of L. Machiels was partially supported by the Fonds National Suisse de la Recherche Scientifique.

## APPENDIX A: $k$-$\epsilon$ EQUATIONS

The modeled equation for the turbulent kinetic energy is obtained from its exact transport equation (cf. Hanjalic and Launder):[34]

$$\frac{\partial k}{\partial t}+\overline{U_i}\,\frac{\partial k}{\partial x_i}=\frac{\partial}{\partial x_i}\left[\left(\frac{\nu_t}{\sigma_k}+\nu\right)\frac{\partial k}{\partial x_i}\right]+\mathfrak{p}-\epsilon, \tag{A1}$$

where $\mathfrak{p}$ is the production of turbulent energy given by

$$\mathfrak{p}=-\overline{u_i u_j}D_{ij}. \tag{A2}$$

The derivation of the modeled $\epsilon$ equation involves many more closure assumptions than the $k$ equation. The modeling of this equation is based on analogies with the $k$ equation and on phenomenological considerations. Its final form is

$$\frac{\partial \epsilon}{\partial t}+\overline{U_i}\,\frac{\partial \epsilon}{\partial x_i}=\frac{\partial}{\partial x_i}\left[\left(\frac{\nu_t}{\sigma_\epsilon}+\nu\right)\frac{\partial \epsilon}{\partial x_i}\right]+C_{\epsilon 1}\,\frac{\epsilon}{k}\,\mathfrak{p}-C_{\epsilon 2}\,\frac{\epsilon^2}{k}. \tag{A3}$$

The two modeled transport equations contain five constants. The values for these coefficients are obtained from experiments for equilibrium turbulent boundary layers and isotropic turbulence. The standard set of constants is

$$C_{\epsilon 1}=1.44,\quad C_{\epsilon 2}=1.92,\quad \sigma_k=1.0,\quad \text{and}\quad \sigma_\epsilon=1.3. \tag{A4}$$

For the $\epsilon$ equation (A3) we do not use the wall damping functions to change the values of constants $C_{\epsilon 1}$ or $C_{\epsilon 2}$, since it is at present not possible to devise a set of functions that mimic the wall variation of the dissipation along the duct perimeter. Also, due to the use of the staggered grid, the value of $k$ is not defined on the wall. Thus, the last two terms in the modeled dissipation equation remain finite. At the wall, the boundary condition for the equations of $k$ and $\epsilon$ were

$$\frac{\partial k}{\partial y}=0\quad \text{or}\quad \frac{\partial k}{\partial z}=0\quad \text{and}\quad \epsilon=\nu\,\frac{\partial^2 k}{\partial y^2}\ \text{or}\ \epsilon=\nu\,\frac{\partial^2 k}{\partial z^2}. \tag{A5}$$

## APPENDIX B: SECOND-MOMENT MODEL

When the full Reynolds stress model (RSM) is used in the present paper, the transport equations to this model were obtained from the model proposed by Gibson and Launder:[10]

$$\frac{\partial \overline{u_i\ u_j}}{\partial t}+\overline{U_k}\,\frac{\partial \overline{u_i\ u_j}}{\partial x_k}=d_{ij}+\mathfrak{p}_{ij}-\frac{2}{3}\,\delta_{ij}\epsilon+\phi_{ij}, \tag{B1}$$

where the term

$$d_{ij}=\frac{\partial}{\partial x_k}\left[\left(C_s\overline{u_k u_l}\,\frac{k}{\epsilon}+\nu\right)\frac{\partial \overline{u_i\ u_j}}{\partial x_k}\right], \tag{B2}$$

models stress diffusion and

$$\mathfrak{p}_{ij}=-\left(\overline{u_i u_k}\,\frac{\partial \overline{U_j}}{\partial x_k}+\overline{u_j u_k}\,\frac{\partial \overline{U_i}}{\partial x_k}\right) \tag{B3}$$

is the exact stress production;

$$\phi_{ij}=\phi_{ij1}+\phi_{ij2}+\phi_{ijw1}+\phi_{ijw2} \tag{B4}$$

represents the pressure–strain interaction, each part modeled by

$$\phi_{ij1}=-C_1\,\frac{\epsilon}{k}\left(\overline{u_i u_j}-\frac{2}{3}\,\delta_{ij}k\right), \tag{B5}$$

$$\phi_{ij2}=-C_2\left(\mathfrak{p}_{ij}-\frac{2}{3}\,\delta_{ij}\mathfrak{p}\right), \tag{B6}$$

$$\phi_{ijw1}=C_1^w\,\frac{\epsilon}{k}\left(\overline{u_k u_m}n_k n_m\delta_{ij}-\frac{3}{2}\,\overline{u_k u_i}n_k n_j-\frac{3}{2}\,\overline{u_k u_j}n_k n_i\right)f, \tag{B7}$$

$$\phi_{ijw2}=C_2^w\left(\phi_{km2}n_k n_m\delta_{ij}-\frac{3}{2}\,\phi_{ik2}n_k n_j-\frac{3}{2}\,\phi_{jk2}n_k n_i\right)f. \tag{B8}$$

The last two terms accounting for the effects of the wall, $n_i$ is the wall–normal unit vector in the direction $i$, and $f=0.4k^{1.5}/\epsilon\,\Delta n$, with $\Delta n$ the wall–normal distance. The values of the constants used in this model are

$$C_s=0.22,\quad C_1=1.8,\quad C_2=0.6,\quad C_1^w=0.5,\quad \text{and}\quad C_2^w=0.3. \tag{B9}$$


[1] C. G. Speziale, ''Analytical methods for the developments of Reynolds-stress closures in turbulence,'' Annu. Rev. Fluid Mech. **23**, 107 (1991).
[2] C. G. Speziale, ''On non-linear $k$-$l$ and $k$-$\epsilon$ models of turbulence,'' J. Fluid Mech. **178**, 459 (1987).
[3] D. D. Joseph, *Fluid Dynamics of Viscoelastic Liquids* (Springer-Verlag, New York, 1984).
[4] T. Shih, J. Zhu, and J. L. Lumley, ''A realizable Reynolds stress algebraic equation model,'' NASA Tech. Memo TM-105993, 1993.
[5] R. Rubinstein and J. M. Barton, ''Nonlinear Reynolds stress models and the renormalization group,'' Phys. Fluids A **8**, 1472 (1990).
[6] A. O. Demuren and W. Rodi, ''Calculation of turbulence-driven secondary motion in non-circular ducts,'' J. Fluid Mech. **140**, 189 (1984).
[7] T. B. Gatski and C. G. Speziale, ''On explicit algebraic stress models for complex turbulent flows,'' J. Fluid Mech. **254**, 59 (1993).
[8] S. B. Pope, ''A more general effective-viscosity hypothesis,'' J. Fluid Mech. **72**, 331 (1975).
[9] A. Huser, S. Biringen, and F. F. Hatay, ''Direct simulation of turbulent flow in a square duct: Reynolds-stress budgets,'' Phys. Fluids **6**, 3144 (1994).
[10] M. M. Gibson and B. E. Launder, ''Ground effects on pressure fluctuations in the atmospheric boundary layer,'' J. Fluid Mech. **86**, 491 (1979).
[11] R. Cheesewright, G. McGrath, and D. G. Petty, ''LDA measurements of turbulent flow in a duct of square cross section at low Reynolds number,'' Aeronautical Engineering Department, University of London, Report No. ER 101, 1990.
[12] A. Huser and S. Biringen, ''Direct numerical simulation of turbulent flow in a square duct,'' J. Fluid Mech. **257**, 65 (1993).
[13] S. Gavrilakis, ''Numerical simulation of low-Reynolds-number turbulent flow through a straight square duct,'' J. Fluid Mech. **244**, 101 (1992).
[14] S. Gavrilakis, ''Turbulent velocity structures derived from POD analyses,'' Institut de Machines Hydrauliques et de Mécanique des Fluides, École Polytechnique Fédérale de Lausanne, Report No. T-93-30, 1993.
[15] R. A. Antonia, J. Kim, and L. W. B. Browne, ''Some characteristics of small-scale turbulence in turbulent duct flow,'' J. Fluid Mech. **233**, 369 (1991).
[16] P. Bradshaw and J. Blair Perot, ''A note on turbulent energy dissipation in viscous wall region,'' Phys. Fluids **5**, 3305 (1993).
[17] J. Kim, P. Moin, and R. Moser, ''Turbulent statistics in fully developed channel flow at low Reynolds number,'' J. Fluid Mech. **177**, 133 (1987).
[18] H. Tennekes and J. L. Lumley, *A First Course in Turbulence* (MIT Press, Cambridge, MA, 1972).
[19] J. L. Lumley, *Computational Modeling of Turbulent Flows*, Advances in

Applied Mechanics (Academic Press, New York, 1978), Vol. 18, p. 123.
[20]S. Gavrilakis, ''Large-scale structures in the turbulent flow near a right-angled corner,'' *1st ERCOFTAC Workshop on Direct and Large-Eddy Simulation*, Surrey, 1994.
[21]F. B. Gessner, ''The origin of secondary flow in turbulent flow along a corner,'' J. Fluid Mech. **58**, 1 (1973).
[22]C. G. Speziale, ''The dissipation rate correlation and turbulent secondary flows in noncircular ducts,'' Trans. Am. Soc. Mech. Eng. J. Fluid Eng. **108**, 118 (1986).
[23]P. A. Durbin, ''Near-wall turbulence closure modeling without damping functions,'' Theor. Comput. Fluid Dyn. **3**, 1 (1991).
[24]W. Rodi and N. N. Mansour, ''Low Reynolds number $k$-$\epsilon$ modeling with the aid of direct simulation,'' J. Fluid Mech. **250**, 509 (1993).
[25]G. Mompean, ''Three-equation turbulence model for prediction of the mean square temperature variance in grid-generated flows and round jets,'' Int. J. Heat Mass Transfer **37**, 1165 (1994).
[26]K. Y. Chien, ''Prediction of channel and boundary-layer flows with a low-Reynolds-number turbulence model,'' AIAA J. **20**, 33 (1982).
[27]C. K. G. Lam and K. Bremhorst, ''A modified form of the $k$-$\epsilon$ model predicting wall turbulence,'' Trans. Am. Soc. Mech. Eng. J. Fluid. Eng. **103**, 456 (1981).
[28]W. C. Reynolds, ''Computation of turbulent flows,'' Annu. Rev. Fluid Mech. **8**, 183 (1976).
[29]P. A. Lindberg (private communication, 1994).
[30]S. Nisizima, ''A numerical study of turbulent square-duct flow using an anisotropic $k$-$\epsilon$ model,'' Theor. Comput. Fluid Dyn. **2**, 61 (1990).
[31]B. E. Launder and D. P. Tselepidakis, ''Contribution to the modelling of near-wall turbulence,'' *Turbulent Shear Flows 8*, edited by F. Durst, R. Friedrich, B. E. Launder, F. W. Schmidt, and J. H. Whitelaw, Munich 1993, p. 81.
[32]N. Naimi and F. B. Gessner, ''A calculation method for developing turbulent flow in rectangular ducts of arbitrary aspect ratio,'' J. Fluid Eng. **117**, 249 (1995).
[33]B. E. Launder, G. J. Reece, and W. Rodi, ''Progress in the development of a Reynolds-stress turbulence closure,'' J. Fluid Mech. **68**, 537 (1975).
[34]K. Hanjalic and B. E. Launder, ''A Reynolds stress model of turbulence and its application to thin shear flows,'' J. Fluid Mech. **52**, 609 (1972).